Tampere University

Santeri Hanhinen

FREQUENCY DOUBLING OF HIGH-POWER SEMICONDUCTOR LASER DIODES USING A PLANAR NONLINEAR CRYSTAL

Bachelor's thesis
Faculty of Engineering and Natural Sciences
November 2021

ABSTRACT

Santeri Hanhinen: Frequency doubling of high-power semiconductor laser diodes using a planar nonlinear crystal
Bachelor's thesis
Tampere University
Bachelor's Degree Program in Science and Engineering
November 2021

Semiconductor laser diodes are at the forefront of scientific research and are very important in everyday life. Wavelengths ranging from infrared to ultraviolet can be produced with the right semiconductor materials and careful planning. Some wavelengths on this bandwidth can not be produced with traditional semiconductor laser diodes with good enough efficiency.

One method of achieving these wavelengths is to use nonlinear materials that can convert some of the incident light to different frequencies. Frequency doubling, where the frequency of the incident light is doubled, is the most interesting nonlinear interaction considering this thesis.

Many nonlinear interactions require high optical intensities in order to occur. This condition sets requirements for both the power and the beam quality of the laser diode used. High-power laser diodes often suffer from less than ideal beam quality. This is hard to optimize but it can be improved with different structures in the laser. In this thesis, the focus was to experiment on how well laser diodes with less than ideal beam quality could be utilized with nonlinear waveguides.

In the theoretical part of this thesis, the focus is on the fundamentals of semiconductors and nonlinear interactions. The experimental side introduces the experimental setup and results that were achieved. The measurements in this thesis were successful in achieving frequency doubling with a high power laser operating at 1154 nm wavelength. The conversion to frequency doubled 577 nm yellow second harmonic beam with a planar nonlinear waveguide was measured to be 14.7 $\%/W/cm^2$ with coupling efficiency of 60 % to the waveguide. These results are very close to the optimum situation reported by the manufacturer of the waveguide. The experiments conducted in this thesis and the results point to future development in beam quality, nonlinear crystals and also in the methods of coupling light in the crystal.

Keywords: LASER, nonlinear material, second-harmonic generation

TIIVISTELMÄ

Santeri Hanhinen: Korkeatehoisen puolijohdelaserin taajuuskahdennus epälineaarisella planaarisella aaltojohteella
Kandidaatintyö
Tampereen yliopisto
Tekniikan ja luonnontieteiden TkK-tutkinto-ohjelma
Marraskuu 2021

Puolijohdelasereilla on valtava merkitys sekä nykypäivän tutkimuksessa että jokapäiväisessä elämässä. Huolellisella suunnittelulla ja oikeilla puolijohdemateriaaleilla voidaan saavuttaa aallonpituuksia infrapuna-alueelta aina ultravioletin alueelle. Joitakin aallonpituuksia tällä aallonpituuskaistalla on kuitenkin vaikea muodostaa perinteisillä puolijohdemateriaaleilla riittävän hyvällä hyötysuhteella.

Yksi mahdollisuus näiden aallonpituuksien saavuttamiseen on käyttää materiaaleja, joilla on epälineaarisia ominaisuuksia. Tällaisten materiaalien erikoisuus piilee niiden kyvyssä muuntaa osa niihin kohdennetusta valosta eri aallonpituuksille. Tämän opinnäytetyön kannalta kiinnostavin epälineaarinen vuorovaikutus on taajuuskahdennus, jossa valon taajuus kaksinkertaistuu eli aallonpituus puolittuu.

Monet epälineaariset vuorovaikutukset vaativat toimiakseen suurta valon intensiteettiä materiaalin sisällä. Kyseinen vaatimus asettaa käytettäville lasereille ehtoja sekä tehon että säteenlaadun kannalta. Korkeatehoiset laserit kuitenkin kärsivät usein heikosta säteenlaadusta. Tätä voidaan parantaa erilaisilla rakenteilla laserissa, mutta optimia on kuitenkin vaikea saavuttaa. Tämän opinnäytetyön painopisteenä on tutkia, miten korkeatehoisia ja säteenlaadultaan ei-ideaalisia puolijohdelasereita voidaan käyttää epälineaaristen materiaalien kanssa taajuuskahdennuksessa.

Työn kirjallisuusosiossa keskitytään sekä puolijohdelasereiden että epälineaaristen vuorovaikutusten toimintaperiaatteisiin. Kokeellisessa osiossa tutustutaan tutkimuksessa käytettyyn laitteistoon sekä esitellään sillä saatuja tuloksia. Tutkimuksissa onnistuttiin saavuttaman taajuuskahdennus suuritehoisella laserdiodilla, jonka aallonpituus on 1154 nm. Taajuuskahdennuksen normalisoitu hyötysuhde mitattiin olevan 14,7 $\%/W/cm^2$ ja kytkentähyötysuhde epälineaariseen planaariseen aaltojohteeseen 60 % . Nämä tulokset ovat hyvin lähellä epälineaarisen aaltojohteen valmistajan ilmoittamaa optimaalista tilannetta. Tässä opinnäytetyössä tehdyt kokeet ja niistä saadut tulokset nostavat esiin tulevat kehityskohteet käytettyjen laserien säteenlaadussa, lasersäteen kytkemisessä aaltojohteeseen sekä epälineaaristen aaltojohteiden kanssa.

Avainsanat: LASER, epälineaariset materiaalit , taajuuskahdennus

CONTENTS

LIST OF SYMBOLS AND ABBREVIATIONS

E_C	conduction band energy level
E_V	valence band energy level
E_f	Fermi energy
E_g	band gap energy
E_{F_C}	conduction band Fermi energy
E_{F_V}	valence band Fermi energy
$I_{2\omega}$	SHG wave intensity
M^2	beam quality factor
N_{Tr}	transparency density
V_f	bias applied
Δk	phase difference
Λ	dbr grating period
$\chi^{(1)}$	linear susceptibility
$\chi^{(2)}$	second order susceptibility
$\chi^{(3)}$	third order susceptibility
λ	wavelength
θ	half-angle beam divergence
f	frequency
l_c	coherence length
n_{eff}	effective refractive index
w_0	beam radius at beam waist
P	polarization wave
DBR	Distributed Bragg-reflector
NCE	Normalized conversion efficiency
NIR	Near-infrared
QPM	Quasi-phase-matching
RWG	Ridge waveguide

SHG	Second-harmonic generation
TAU	Tampere University
TUNI	Tampere Universities

1. INTRODUCTION

Semiconductor laser diodes are at the forefront of scientific research and have still huge development potential. Certain wavelengths can not be produced with traditional semiconductor laser diodes and these wavelengths require additional equipment to reach. Furthermore, high-power laser diodes often suffer from less than ideal beam quality.

One method of achieving these wavelengths is to use nonlinear materials that can convert some of the incident light to different frequencies. In order to reach high frequencies, one could use nonlinear materials that have a tendency for frequency doubling or halving the wavelength of the incident laser beam. The devices constructed from these nonlinear materials can require very tight focusing of the beam and good beam quality to achieve useful conversion to the shorter wavelengths. In this thesis, the focus was to experiment on how well laser diodes with less than ideal beam quality could be utilized with nonlinear waveguides.

The explanation of the theory behind this thesis starts in chapter 2. Chapter 2 begins with the basics of laser operation followed by some key laser diode structures used in the experimental part of this thesis. Thirdly in chapter 2, laser beam quality is examined and after that we introduce the theory governing nonlinear interactions and second-harmonic generation (SHG). In chapter 3, the results of previous research about SHG with high-power lasers is briefly discussed to set comparison points to the research done in this thesis. After that in chapter 3, the experimental methods are explained and the results from the experiments are analysed. Chapter 4 summarizes the thesis' results.

2. THEORY

The basic fundamentals and theories of this thesis subject matter are covered in this chapter. Section 2.1 introduces the principles of semiconductor laser operation and section 2.2 focuses on three different structures for laser devices that may be utilized to achieve desired properties for the output beam. In section 2.3, the factors of beam quality are inspected and lastly, section 2.4 explains the basic theory of nonlinear interactions and second-harmonic generation with laser light in a periodically poled nonlinear crystal.

2.1 Basics of semiconductor lasers

Semiconductor lasers are solid-state lasers and the materials for them are mostly from the third and the fifth group of the periodic table (III-V compounds). The laser operation occurs in an active medium. The active medium is located inside of a cavity resonator which provides feedback to the active medium. More energy is pumped in the active medium by a pumping process, either optical or electrical. This basic structure for a semiconductor laser is illustrated in figure 2.1.

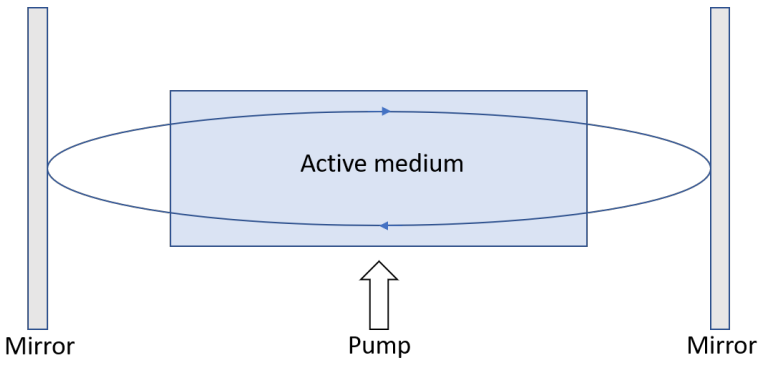

Figure 2.1. *Basic laser schematic*

Semiconductor lasers are widely used because they are reliable, efficient, economical to mass produce and can produce a high quality light beam in a large range of wavelengths.

2.1.1 Basics for gain in semiconductors

Allowed energies for electrons in semiconductors can be calculated using Bloch's theorem and solving the Schrödinger equation in the crystalline structure of semiconductors [1]. The solutions form the band structure of allowed electron energy bands and the bands are separated by band gap energy E_g. At absolute zero temperature, $T = 0\,K$, the highest occupied energy for electrons is the Fermi energy E_F. The highest occupied energy band is called the valence band and the lowest unoccupied energy band is called the conduction band. For semiconductor lasers, the active medium is direct gap material meaning that the top of the valence band and the bottom of the conduction band have the same wavevector value k [2]. This facilitates for strong interaction with light. [3].

If enough energy is added to the system, electrons can be raised from the valence band to the conduction band. The energy added, in linear processes, needs to exceed the bandgap energy between the valence and the conduction band i.e. $\Delta E \geq E_g$. The electrons excited to the conduction band thermalize quickly $(\leq 1ps)$ to the lowest possible unoccupied energy levels in the conduction band due to non-radiative decay [2]. Similar intraband transition happens in the valence band, where electrons occupy the lowest possible energy states, leaving unoccupied energy levels at the top of the valence band, called holes [2]. The electrons pumped to the conduction band can then fall back to the valence band combining with the holes at the top of the valence band. This process of spontaneous emission results in light emission in a random spatial direction [4]. A simple band structure of valence and conduction band is illustrated in figure 2.2.

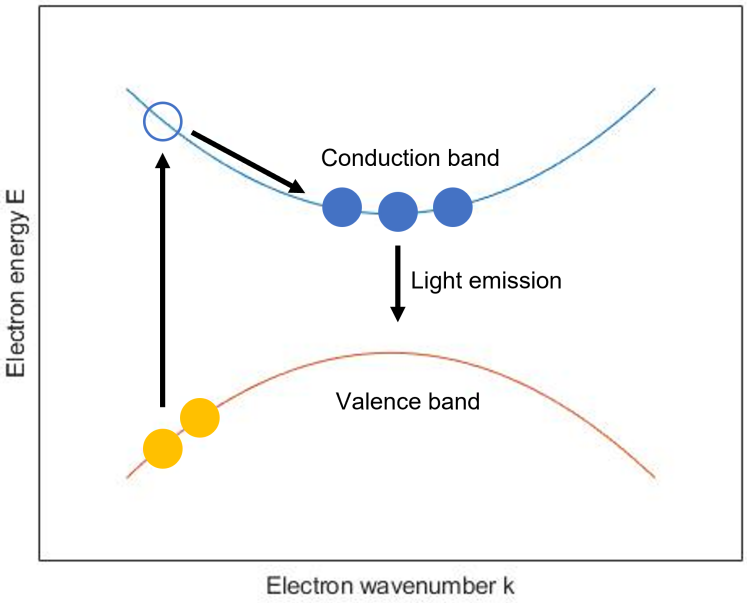

Figure 2.2. *Simple explanation of light emission in semiconductor with direct bandgap. Adapted from [4].*

The interband transition that occurs when electrons and holes recombine takes considerably more time ($\approx 1ns$) than intraband transitions. This means that even in non-equilibrium conditions, the holes in the valence band are in equilibrium with each other and so are the electrons in the valence band. Because of this, it is appropriate to introduce quasi-Fermi energies: E_{F_V},E_{F_C}, subsequently for valence and conduction bands [1]. The quasi-Fermi energies are the highest occupied energy states in both conductive band and the valence band at $T = 0\,K$. These energies are dependent on the number density N of carriers excited to the conductive band; E_{F_V} increases and E_{F_C} decreases while N increases. The quasi-Fermi energies are then better denoted as $E_{F_V}(N)$,$E_{F_C}(N)$. [2]

Incident photons can be absorbed and excite electrons from the valence band to the conduction band or stimulate a recombination of a electron and a hole. Stimulated emission results in amplifying, as in duplicating, the original incident photon rather than emitting in a random spatial direction. [1] At thermal equilibrium, the transition probability for absorption is higher than for stimulated emission [5]. To achieve positive net positive gain g in the semiconductor the conditions need to favor stimulated emission rather than absorption. The probabilities for absorption and stimulated emission are dependent on the density of carries in the valence band and in the conduction band.[2] With pumping processes, electrons can be raised to the conduction band resulting in higher probabilities of stimulated emission [5]. Electrons excited to the conduction band result in the change in both $E_{F_V}(N)$ and $E_{F_C}(N)$ and the condition for positive net gain is presented as [2]:

$$E_g \leq hf \leq E_{F_V}(N) - E_{F_C}(N). \tag{2.1}$$

This condition is called population inversion. The boundary condition, where the bandgap energy E_g equals the difference of the quasi-Fermi energies is called the transparency condition and the corresponding injected carrier density is the transparency density N_{Tr} [2]. At transparency, the gain for an incident photon with energy that equals E_g is zero. If the injected carrier density is greater than the transparency density, positive net gain can occur for photons with energies between E_g and $E_{F_V}(N)-E_{F_C}(N)$.

2.1.2 The p-n semiconductor junction

The electrical properties of semiconductor materials are directly tied to the number of free carriers in the crystalline structure. In a pure semiconductor, the number of electrons and holes as free carriers is exactly the same because free carriers can only be created from covalent -bond breakage and this process creates pairs of electrons and holes. [6]. The electric properties of semiconductor materials can be altered by introducing impurity atoms to the crystalline structure [1]. Semiconductors that have some of the atoms in the lattice replaced by an impurity atoms, are called doped semiconductors. Impurity atoms can introduce free carriers as electrons or as holes. The process of introducing impurity

atoms that provide free electrons to the lattice is called N-doping and introducing free holes is called P-doping. N-doped materials can donate electrons and P-doped materials can accept electrons. In the n-type semiconductor, the Fermi energy E_F is raised to the conduction band because of the excess electrons and in the p-type semiconductor, the Fermi energy drops to the valence band.

Attaching a p-type semiconductor with a n-type semiconductor forms a P-N junction. P-N junctions are used widely in solid-state electronics and lasers utilize the P-N junction to generate coherent light. After forming the junction and with no applied voltage, free carriers begin diffusing across the junction. Electrons diffuse from the n-side to p-side and some of them combine with holes, leaving behind positively charged ions that are attached to the lattice structure. Holes diffuse from the p-side to the n-side combining with electrons, leaving behind negatively charged ions. This creates an area in the junction that is depleted of mobile carriers. Any free charge carries that enter this area, experience the force from the formed electric field in the area and start drifting depending on the charge. At equilibrium, the diffusion current and the drift current are equal but to opposite directions.[1] The equilibrium state of a p-n junction without voltage applied can be seen in figure 2.3

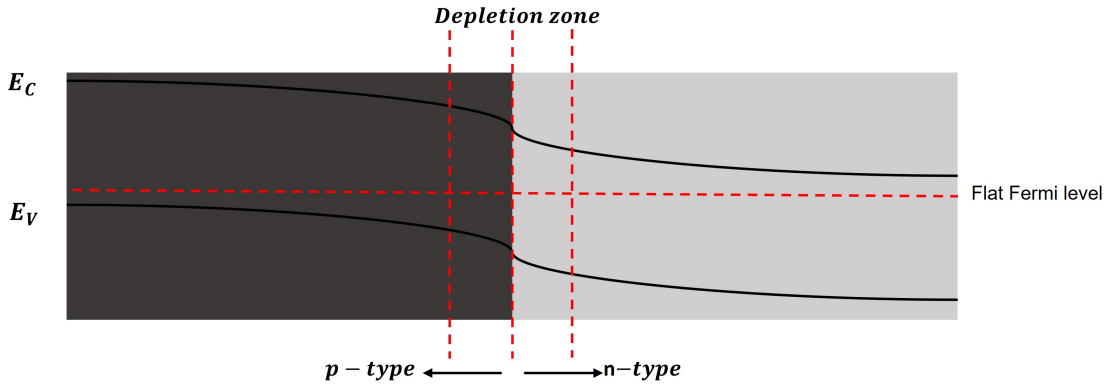

Figure 2.3. *P-N junction with no voltage applied. Adapted from [1].*

E_C is the conduction band energy level E_V is the valence band energy level. The Fermi energies for both n-side and p-side are seen to be the same as in figure 2.3 when both n-side and p-side are in thermal equilibrium. Applying bias V_f to the junction changes the energy difference ΔE between the two energies by eV_f. The energy difference can decrease or increase depending on the applied voltage. With a forward bias, the energy difference decreases and with a reverse bias, the energy difference increases as seen in figure 2.4. [1]

In the case of forward biasing, the applied voltage shrinks the depletion zone and the flow of carriers increases. This means that electrons and holes are injected in the junction area.

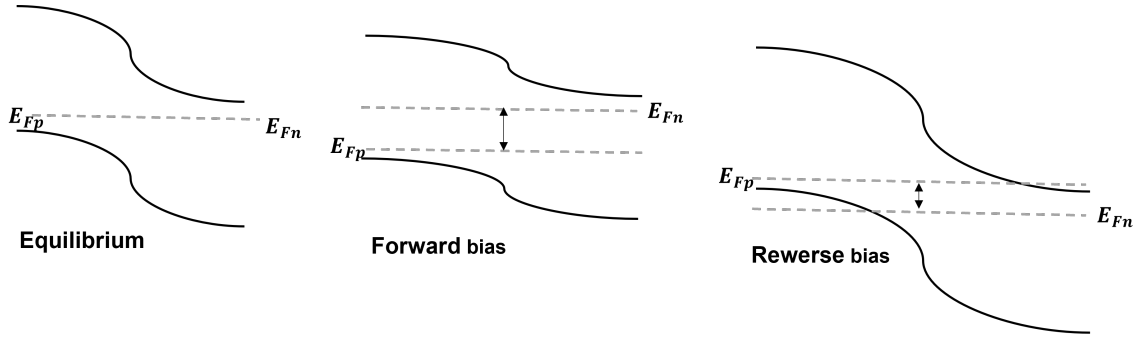

Figure 2.4. *P-N junction energy band with different bias . Adapted from [1].*

As discussed in section 2.1.1, the electrons in the conduction band recombine with the holes in the valence band to generate light emission. The limiting case for incident light to stimulate the recombination rather than to be absorbed was to reach population inversion of the carriers. With appropriate voltage applied, this condition can be reached and lasing can occur.

2.2 Laser structure

There are many different types of semiconductor laser diodes and they all have their different uses. We are going to focus on edge-emitting lasers. Edge-emitting semiconductor lasers emit light along the plane of the semiconductor wafer as seen in figure 2.5.

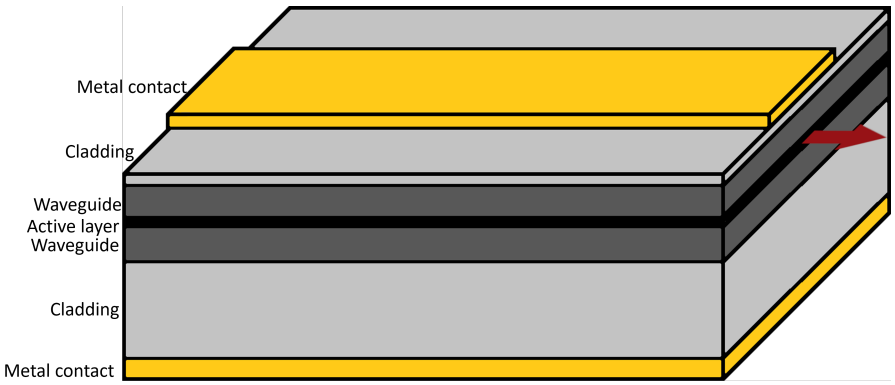

Figure 2.5. *Cross-section of edge-emitting laser. Adapted from [3].*

Edge-emitting lasers are typically constructed with several different regions. Most basic structures would only have the active gain medium in a cavity surrounded by two mirrors as in figure 2.1. However, to achieve different properties for the laser beam, several different structures can be added. These structures can be used to achieve for example narrower emitted spectral line-width, improved beam quality and increased optical power

2.2.1 Distributed Bragg reflector

One or both of the mirrors at ends of the laser cavity can be replaced by Bragg grating mirrors. These mirrors form the basis for the distributed Bragg reflector lasers (DBR-lasers). These sections of the laser are typically passive, meaning that the area is not under any pumping process. The main reason to use Bragg grating mirrors over regular laser mirrors, is to achieve good frequency selectivity.

The frequency selectivity of Bragg mirrors arises from their periodic grating structure and Bragg reflections caused by it. The grating is constructed from materials that have varying index of reflection. In the case where lateral dimensions of the Bragg reflector are not taken into consideration, the length of the grating and the difference between the index of refraction of the materials used in the grating determine the total reflectivity of the mirror. The period of the grating Λ can be calculated for the desired wavelength λ as in [2]:

$$\Lambda = \frac{\lambda}{2 < n_{eff} >}, \tag{2.2}$$

where $< n_{eff} >$ is the average effective refractive index of the grating along the gratings length. As can be seen from equation 2.2, there is only a single wavelength that satisfies this equation with a fixed period Λ. This means that a well designed distributed Bragg reflector filters out a very narrow linewidth of frequencies (Bragg frequency) that are reflected back constructively as seen in figure 2.6.

In figure 2.6, the wave is incident from the right side and the grating is designed for 800 nm light. This grating in a edge-emitting laser can be made by etching a periodic pattern into the area that is wanted to be used as a Bragg mirror. This etched grating can then be filled with a material that has a different refraction index resulting in a grating period like mentioned before.

2.2.2 Ridge waveguide

Waveguides are used in laser diodes to confine the beam in lateral and transverse directions. Good confinement over the length of the laser cavity essentially removes beam divergence. Confinement in the active area of the laser results in high optical intensities in the waveguide and improves the modal gain in the active material. [8]

Ridge waveguides are used to improve both lateral confinement and so to limit the RWG to lase at a single spatial mode. [8] An illustration of ridge waveguide is in figure 2.7.

This type of ridge-waveguide is easier to fabricate than to have the waveguide buried. RWG stuctures also allow for higher power applications because of low current confinement. [10]

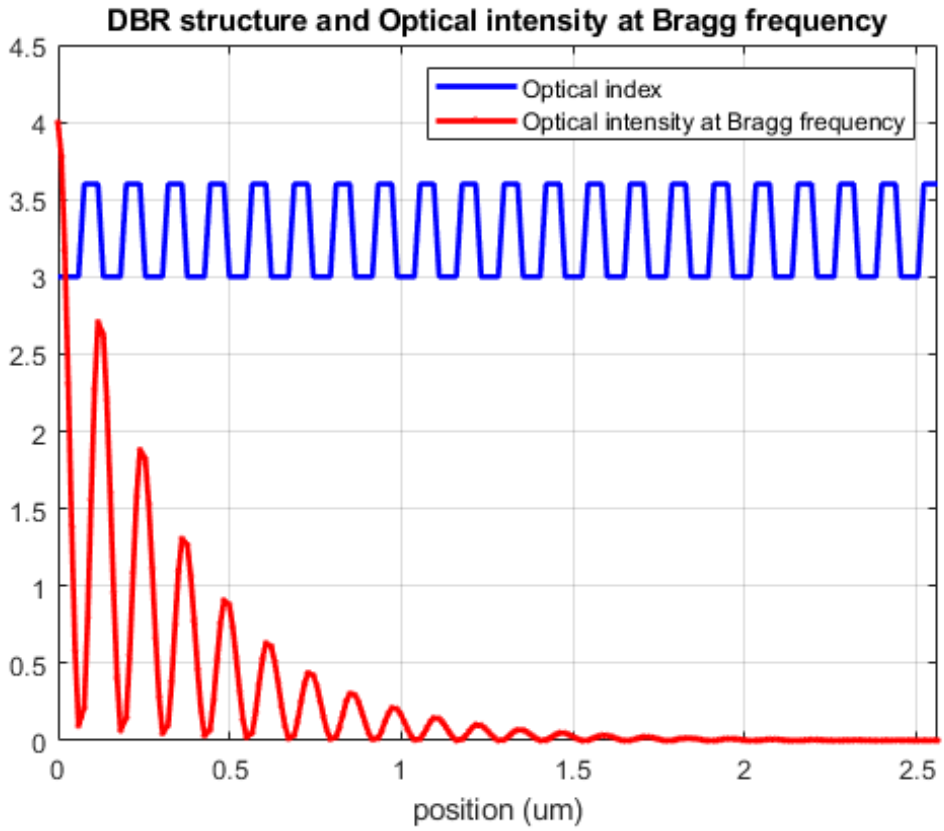

Figure 2.6. *Bragg mirror operation for different wavelengths. Adapted from [7].*

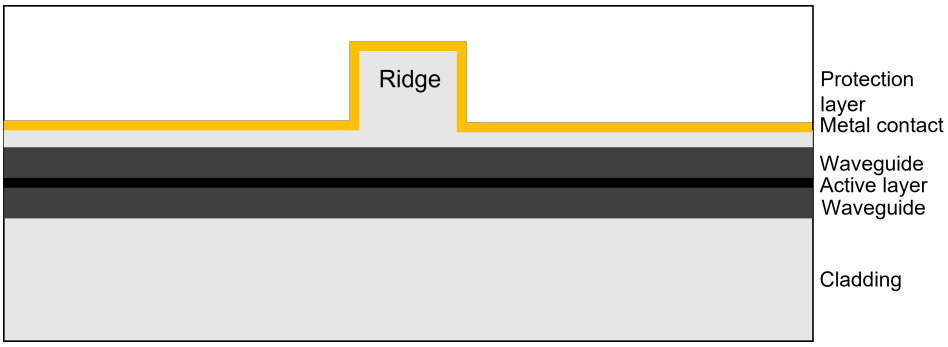

Figure 2.7. *Illustration of ridge-waveguide. Adapted from [9].*

2.2.3 Tapered waveguide

To further amplify the optical power of the edge-emitting laser, the waveguide used can be gradually made wider. By making the end facet of the laser wide, it is more resistant to heat damage caused by of optical absorption at the facet [10]. A simplified illustration of the tapered section can be seen in figure 2.8.

The transverse mode of the beam is kept the same in the tapered section and the beam expands in the tapered section by diffraction [10].

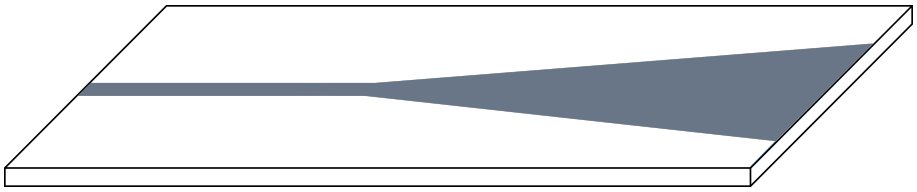

Figure 2.8. *Simplified illustration of tapered section of laser diode. Adapted from [11].*

2.3 Beam quality

The beam quality parameter or the M^2 factor, is one of the most commonly used characteristic of laser beams. The M^2 factor describes how close is the beam to the ideal fundamental Gaussian beam. M^2 factor also defines the divergence of the beam. This value can be calculated as in [12]:

$$M^2 = \frac{\lambda}{\pi w_0 \theta}, \tag{2.3}$$

where θ is half-angle beam divergence, w_0 is the beam radius at the beam waist and λ the wavelength. The M^2 factor of one equals the diffraction limited case of a Gaussian beam. This is also theoretically the lowest value for a real beam. [2]

2.4 Nonlinear interactions and materials

Many applications require high-power light that also has a short wavelength. Shorter wavelengths can not be produced with laser diodes with good enough efficiency so one needs to find a way to generate these using different methods. Nonlinear interactions can be used to achieve wavelengths beyond what is possible with regular lasers by using for example frequency-mixing.

2.4.1 Second-harmonic generation

Typically, materials interact with electromagnetic waves in a linear manner. This means that the polarization caused by the fundamental EM wave causes a linear polarization wave in the material. This polarization wave then has the same frequency as the original EM wave. The magnitude of the polarization wave P induced by the EM wave per unit volume in any material can be written as [13]

$$\mathbf{P} = \epsilon_0 \chi^{(1)} \mathbf{E} + \epsilon_0 \chi^{(2)} \mathbf{EE} + \epsilon_0 \chi^{(3)} \mathbf{EEE} + ..., \tag{2.4}$$

where $\mathbf{E}$ is the magnitude of the applied EM field, ϵ_0 is the permittivity of free space and $\chi^{(1)}$ represents the linear susceptibility of the material. The second and third order nonlinear susceptibilities $\chi^{(2)}$ and $\chi^{(3)}$ are responsible for the lower order nonlinear ef-

fects. Second order nonlinearities include for example frequency doubling and sum and difference frequency generation. The Kerr effect arises from the third order nonlinearity. [13]

The dielectric polarization caused by EM fields in a material can be usually approximated to be linear but with high power EM fields this approximation does not hold and the original EM field produces nonlinear dielectric polarization waves in the material. In frequency doubling, a high intensity electromagnetic field, in this case laser beam, generates in a nonlinear material a forced nonlinear polarization wave that has twice the frequency of the fundamental wave. The second order nonlinear suspectibility $\chi^{(2)}$ of the material is responsible for this interaction. So a material that has high second order nonlinear suspectibility $\chi^{(2)}$, is better suited for frequency doubling. [13] Materials that lack high lattice-symmetry can typically be used to achieve $\chi^{(2)}$ nonlinearity. [14]

According to Maxwell's equations, this forced polarization wave radiated a free EM field, a second-harmonic wave, at this doubled frequency (half the wavelength). [13] The fundamental wave and the secondary harmonic wave travel at different phase velocities and gain a phase difference Δk [13]:

$$\Delta k = \frac{4\pi}{\lambda_0}(n_\omega - n_{2\omega}), \tag{2.5}$$

where λ_0 is the fundamental EM fields wavelength and n_ω and $n_{2\omega}$ are the refractive indices for the fundamental frequency and the doubled frequency respectively.

The sign of power flow between these two waves depends on the relative phase difference. After a distance called coherence length l_c, the sign changes and the power starts flowing from the second harmonic wave back to the fundamental wave. The effect of the coherence length can be seen in figure 2.9.

In this figure, the conversion efficiency of the nonlinear material from the fundamental wave to the second-harmonic wave can be seen in the y-axis. Crystal length in the x-axis is the length of the nonlinear crystal. With infinite coherence length, the conversion would continue growing along the length of propagation in a nonlinear crystal. With smaller coherent lengths, yellow graph being the smallest, the conversion can be seen to oscillate between a maximum and zero after every two coherence lengths.

2.4.2 Quasi-Phasematching

To have the power flow constantly from the fundamental wave to the secondary wave, a method called quasi-phase-matching (QPM) is used in the nonlinear waveguide in these experiments.

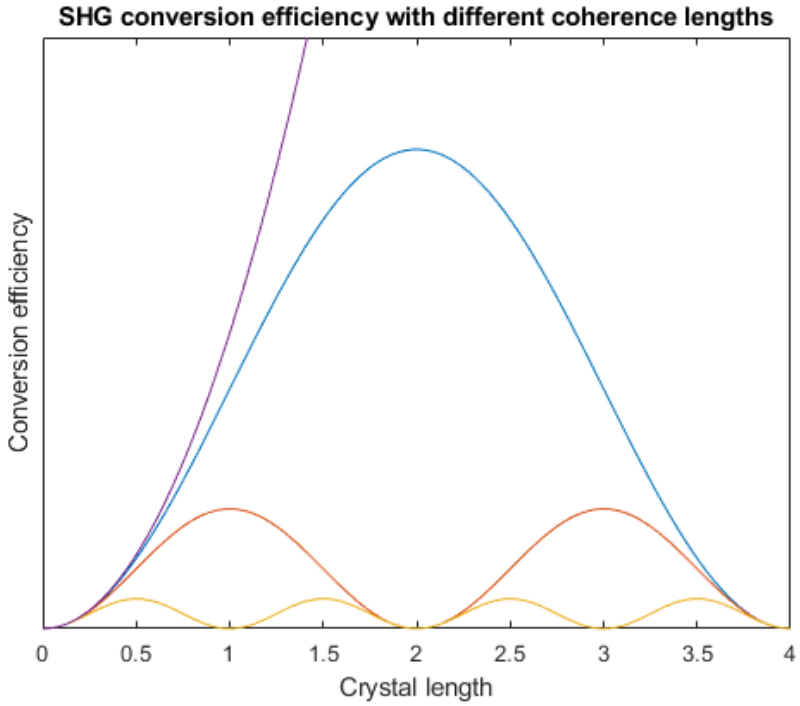

Figure 2.9. *Conversion efficiency dependency on the coherence length. Adapted from [13].*

What this means is that after the coherence length, the relative phase difference is shifted by π and therefore a proper phase difference is maintained. This phase correction can be done by changing the polarization domain in a ferroelectric crystal. And if the nonlinear crystal is periodically poled in a way where the polarization changes every coherence length, we get increasing power. [13] This effect of change of polarization can be seen in figure 2.10.

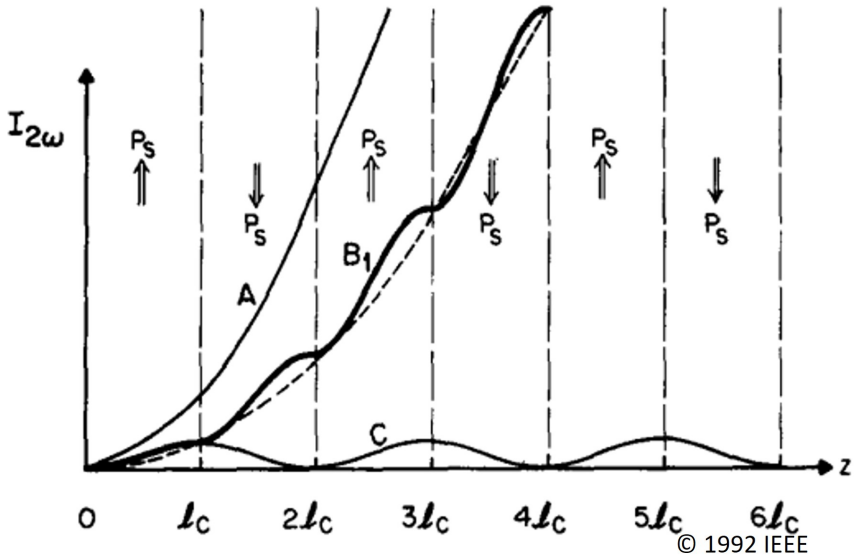

Figure 2.10. *Importance of of periodic pooling in nonlinear crystals. [15]*

In figure 2.10, $I_{2\omega}$ can be seen as the intensity of the second-harmonic wave in the nonlinear material. X-axis shows the propagation in the material. Curve A represents the situation where the two waves are perfectly phase-matched. Curve B is the situation with QPM, where there is a change in the polarization every coherence length. When the two waves are only partially phase-matched, the intensity of the second-harmonic wave oscillates as in curve C. The phase difference can be fine-tuned by changing the temperature of the nonlinear crystal. This changes the refractive index of the material but also the grating period and length of the crystal. [16]

3. EXPERIMENTAL

The experimental research conducted in this work and by previous research groups is laid out in this chapter. Section 3.1 introduces the experimental results of different research groups to use for comparison later on. In section 3.2 the experimental setup that was used in this work is introduced in detail followed by section 3.3 where the measurement process is described. Lastly, in section 3.4 the experimental results gathered from the measurement process are shown and explained.

3.1 Previous results

Frequency doubling of high power lasers has been studied previously with good results. The work done by Daniel Jedrzejczyk et al [17] has the same starting points as the experiments conducted in this work. The results they were able to gather, give a good reference point for these experiments. Most importantly, the results by Daniel Jedrzejczyk et al. from the temperature scan to find the phase-matching temperature to achieve the highest conversion efficiency are in figure 3.1.

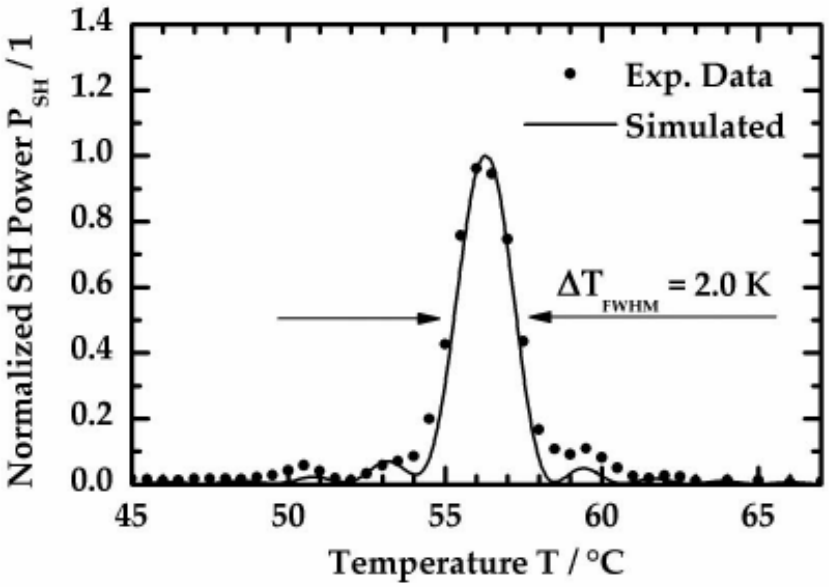

Figure 3.1. *Experimental and simulated results of SHG power dependence on crystal temperature. [17]*

These results should give a good staring point on what to look for when doing the experiments and also what the end results should look like.

3.2 Experimental setup

For these experiments, two slightly modified setups were used. The need to modify the setup arises from using two different laser sources for the experiments. The laser that was used in the first part of the experiments had a desirable wavelength for SHG, stigmatic beam shape and overall good beam quality. This setup can be seen in figure 3.2.

Figure 3.2. *Setup used in experiments with RWG-DBR laser. 1. Collimation lens 2. RWG-DBR laser 3. Neutral density filter 4. Isolator 5. Wave plate 6. SA focusing lens 7. FA focusing lens 8. Nonlinear crystal 9. Crystal oven 10. Focusing lens for yellow light 11. Longpass dichroic mirror 12.Shortpass filter 13. Off picture is power meter.*

In the first part of the experiments, the near infrared (NIR) light source had two different sections. One being a passive DBR-section and the second one was an active RWG section. The RWG section was under $I = 1400mA$ bias in this experiment and the laser was kept at a temperature of $T = 40C$. The NIR light source is placed on a stage that can be moved horizontally. This can be seen at the far left centre of figure 3.2. This movement was crucial because the beam needed to hit the face of the nonlinear waveguide very accurately. The laser can be driven on a constant current using laser diode drivers. This setup has the possibility to use two separate drivers to use different bias on different sections of the lasers. The output beam from the laser was collimated using an aspheric lens (f=4.5mm). This setup only required one collimation lens because the laser the beam was stigmatic. Polarization-depended isolator was used in front of the

laser to prevent back reflections from the optics. Half-wave plate was used to rotate the polarization of the beam to match the polarization of the waveguide. To control the NIR output power, neutral density filter was used. For focusing the beam in the SA-direction, plano-convex cylindrical lens (f=40mm) was used and in the FA direction an aspheric lens (f=8mm) was used. To collect all of the converted yellow light and to block out any NIR light, a set of lenses and mirrors were used. Because the yellow light diverges very quickly, a pre-focus plano-convex lens (f=35mm) was used to collect all of the yellow light. The yellow light was separated from the NIR light by using a longpass dichroic mirror, which let the NIR light pass through and reflected the yellow light. To ensure that all the NIR light was blocked from entering the power meter, shortpass filter was used to filter the beam. The power of the yellow light was measured with a optical power meter and a silicon measurement head.

The second laser that was used had a different structure. This laser also had a desirable wavelength for SHG, good beam quality but the beam was slightly astigmatic. This laser had a passive DBR section, active RWG section and an active tapered section. The laser was operated at 25 ℃ and a bias of 3500 mA was applied to the tapered section and bias of 300 mA was applied to the RWG section. With this current applied, the NIR output power was measured to be 634 mW and the M^2 value was 1.29 for the FA-direction and 4.6 for the SA-direction. The M2 value for the SA-direction is quite large but the intention was to first maximize the coupling in the waveguide in the FA-direction and then optimize the SA-direction inside the waveguide. These differences in the lasers called for slight adjustments in the setup that was used.

The setup was also changed because the laser and the collimating lenses were assembled together on a copper block. So the FA-collimating lens was not needed in this part of the experiments. The laser and the collimating lenses can be seen assembled on the copper block in figure 3.3.

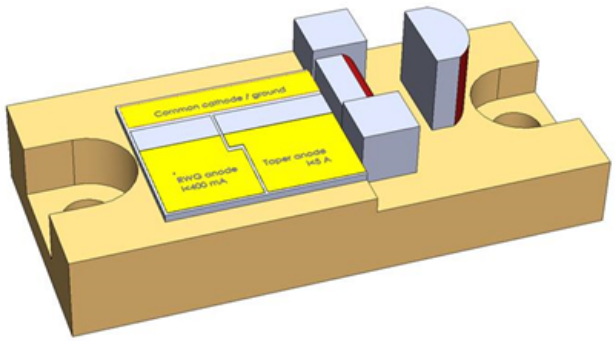

Figure 3.3. *Assembled laser and collimating lenses used in experiments. Illustration by Topi Uusitalo.*

Also the optimal lens distances were simulated to be much longer than in the previous experiments. The optimal distance for the FA-collimating lens and FA-focusing lens was simulated to be 1000mm. The distance is longer because this laser had a slightly larger FA near field than the RWG-DBR laser. Because of the near field, the focusing needs to be tighter and thus longer distance is needed with the lenses that were available for use. Two mirrors were used to change the distance more easily. With this setup, the distance could be changed from 500mm to 1000mm. At these distances, the beam diverged in the SA-direction so much that a pre-focus lens was needed to slightly focus the beam in the SA-direction. The resulting setup can be seen in figure 3.4.

Figure 3.4. *Second setup used in experiments with different lens configuration. 1. Assembly of figure 3.3 2. Isolator 3. Neutral density filter 4. Pre-focus lens 5. Waveplate 6. Mirrors 7. SA focusing lens 8. FA focusing lens 9. Nonlinear crystal 10. Crystal oven 11. Focusing lens for yellow light 12. Longpass dichroic mirror 13. Shortpass filter 14. Power meter*

The positions for the mirrors and the pre-focusing lens was determined by experimenting with different configurations. The best result was achieved when the distance between the FA lenses was 750 mm and the distance of the pre-focus lens from the FA-collimating lens was 250 mm.

The device to achieve frequency doubling and SHG used in these experiments was a periodically poled and MgO doped LiNbO3 (ppMgO:LN) planar waveguide. This waveguide was designed to convert 1154 nm NIR light with SHG to 577 nm yellow light. The phase matching temperature to achieve SHG was given as $40 \pm 20C$. The maximum

coupling efficiency was given to be 70 % and the normalized conversion efficiency as 13 $\%W/cm^2$. Normalized conversion efficiency essentially indicates the crystals performance. To reach the phase matching temperature, a temperature controller and a crystal oven were used. The oven had a teflon cover for temperature insulation but because of the focusing condition of the lenses, this cover could not be used in the experiments. To control the location of the waveguide, the oven was placed on a linear stage that allowed motion perpendicular to the beam. Basic front view of the waveguide can be seen in figure 3.5.

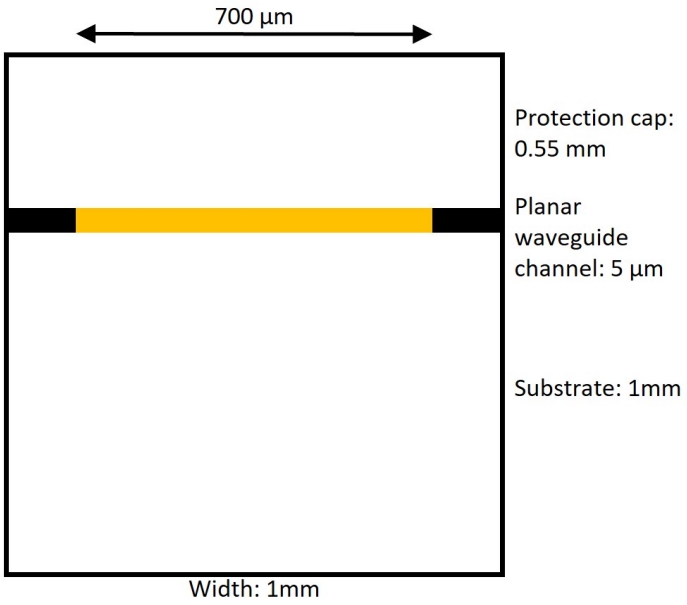

Figure 3.5. *Front view of the waveguide*

The planar waveguide 5 um tall and the poled area is 700 um wide. Because of this, the beam quality of the laser beam had to be good in the FA- direction . Beam quality in the SA- direction also matters because the M^2 factor affects the focusing of the beam.

3.3 Measurement process

Firstly, the laser beam is collimated, in the case of the laser diode, with the aspheric lens. In the second step, the laser beam is aligned with the front facet of the nonlinear crystal. This can be done by adjusting the locations of the collimation lens, the linear stage of the crystal and the laser diode. In the next step, the focusing lenses are placed in front of the nonlinear crystal. Simulation software was used to to find the optimal placements for the focusing lenses. After this, the correct focusing and placement of the laser beam in the nonlinear crystal has to be optimized. The initial placement of the laser beam can be roughly set by using a microscope camera to observe the beam at the back facet of the nonlinear crystal. The optimal focusing and the placement of the beam in the crystal are very hard to optimize because they have to be precise. When it was clear that the beam

was coupled in the waveguide, meaning that yellow light could be seen emitting from the waveguide, the temperature of the waveguide could be changed to find the phase-matching temperature. This was done by changing the crystal ovens temperature and optimizing the lens positions for each temperature. This was necessary since changes in the temperature of the crystal altered the position of the waveguide due to thermal expansion. The optimal location was found when the optical power of yellow light was maximized. It was crucial to keep the NIR power low that hit the face of the crystal since changes in the position of the beam with high power can result in damaging the waveguide.

3.4 Experimental results

For both lasers that were used, the measurements were quite similar. With the RWG-DBR laser, the phase matching temperature was known beforehand so the measurements were made close to that temperature and the results can be seen in figure 3.6.

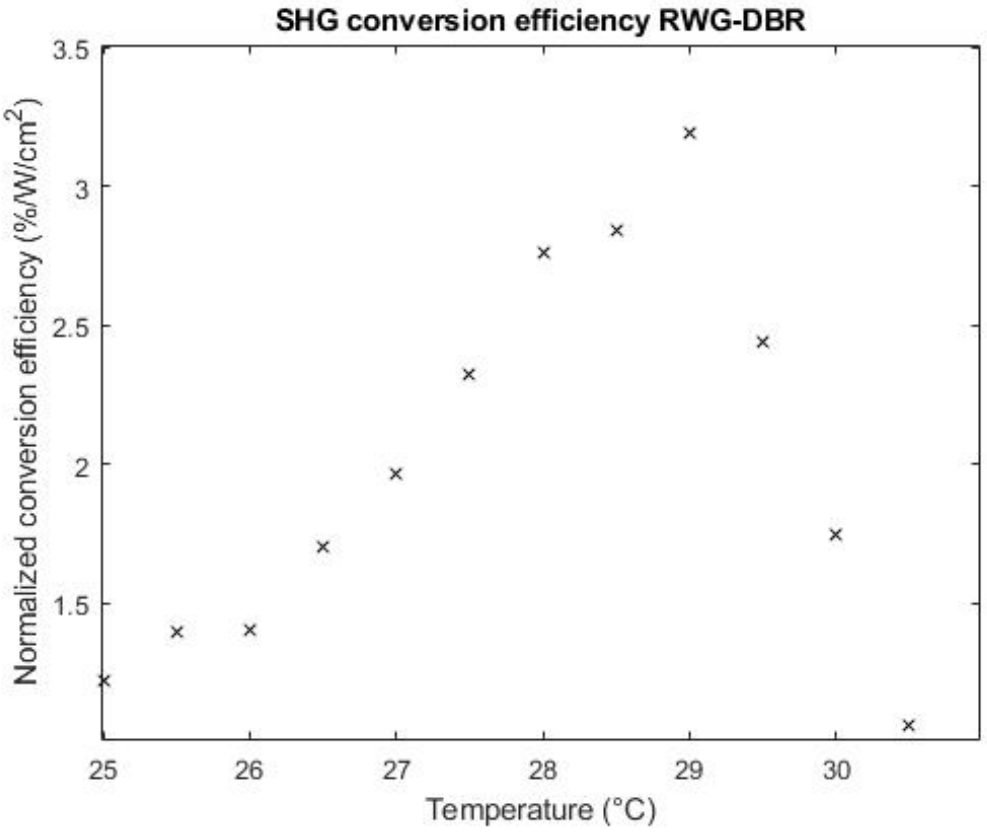

Figure 3.6. *Conversion efficiency of SHG using RWG-DBR laser*

The conversion efficiency in figure 3.6 is calculated without taking into consideration how much of the IR-light gets coupled into the crystal. This coupling percentage was measured to be around 60 percent. This was measured by measuring the IR- power before the crystal and after the crystal using a optical power meter with InGaas optical power

measurement head. The result with the corrected conversion efficiency is seen in figure 3.7.

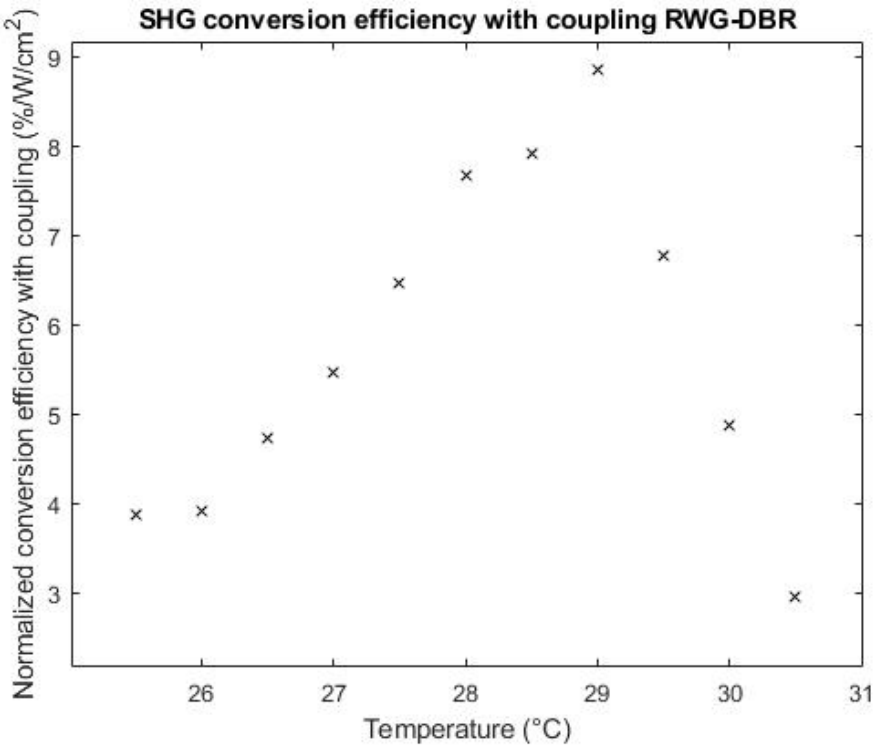

Figure 3.7. *Conversion efficiency of SHG using RWG-DBR laser*

The same measurements were made with the tapered-DBR laser. With this laser the optimal temperature was unknown. Because of this, the range of temperatures in figures 3.8 and 3.9 is larger. The results of the measurements and conversion efficiency is plotted in figure 3.8.

The conversion efficiency in figure 3.8 is once again calculated without the coupling condition. The coupling percentage was also around 60 percent for these measurements. The result with the corrected conversion efficiency is seen in figure 3.9.

Because of the narrow temperature range in figures 3.6 and 3.7, the results are harder to compare with figure 3.1. But the narrow peak can be seen along with the quick drop off in the conversion efficiency. The shape of the curve in figure 3.9 can be seen to resemble the measurement results of previous work done by Jedrzejczyk et al. in figure 3.1. The highest conversion efficiency peak can be seen to be very narrow with a fast drop off when the temperature is changed around the phase-matching temperature.

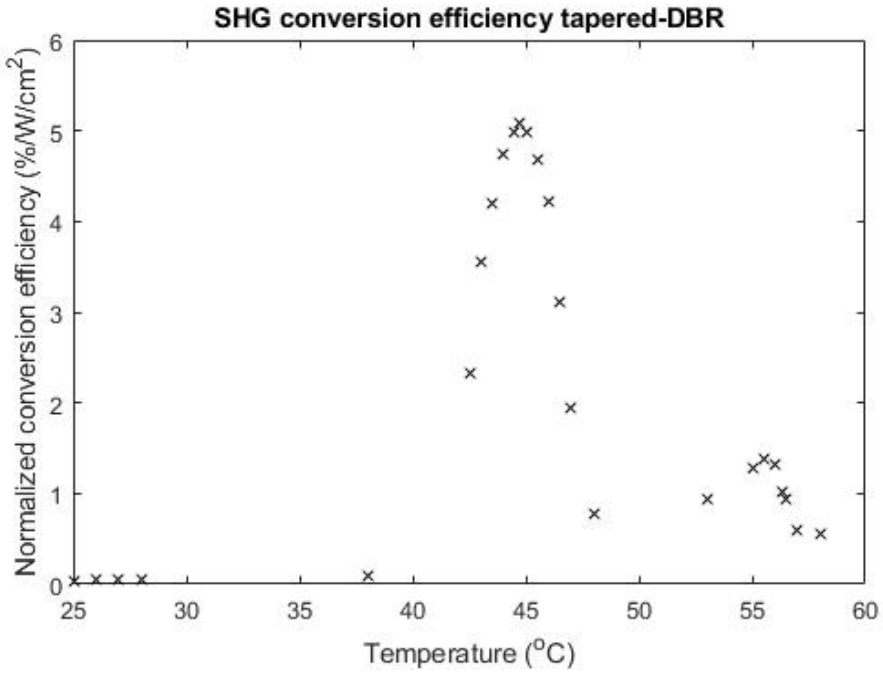

Figure 3.8. *Conversion efficiency of SHG using tapered DBR laser*

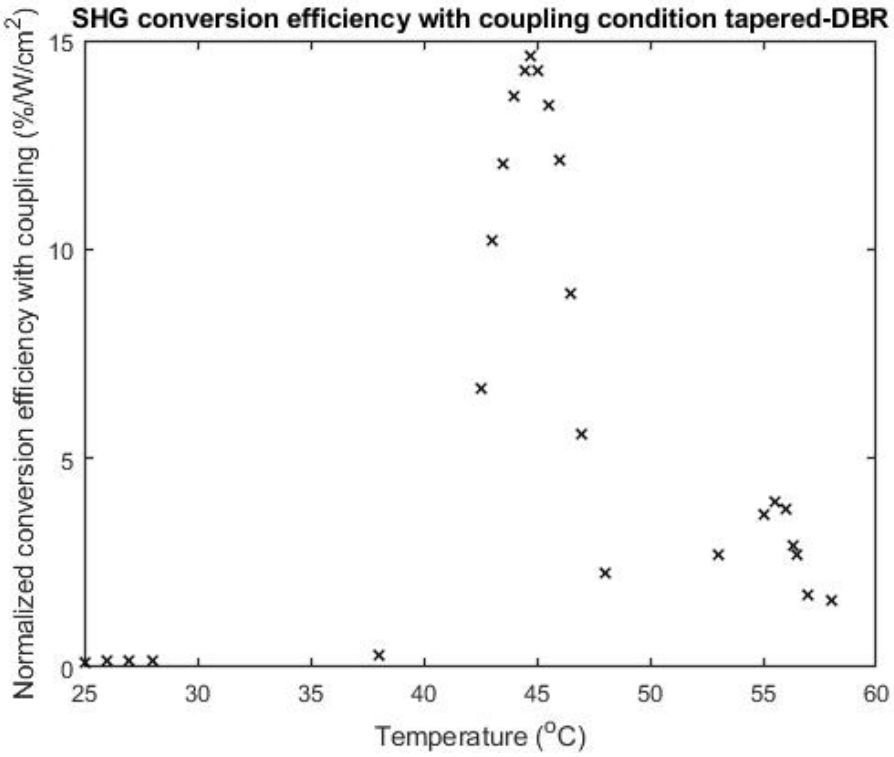

Figure 3.9. *Conversion efficiency of SHG with coupling condition using tapered DBR laser*

4. SUMMARY

The main idea behind this thesis was to experiment with nonlinear interactions, more precisely frequency doubling, using a high power edge-emitting laser diode. The basis for laser action and basic laser structures were introduced to have a better understanding of the experimental setup used. Additionally, the basic theory for frequency doubling was shortly explained. The experiments were conducted with a planar nonlinear waveguide crystal that had not been tested previously in our research group. The main interest was in the conversion efficiency of the crystal and the temperature response that it had to the laser diodes used.

Compared to previous results y Daniel Jedrzejczyk et al [8], the RWG-DBR laser did not show any significant outcome. The results with tapered-DBR however match the previous results quite well and the conversion efficiency is very close to the maximum efficiency that was stated by the manufacturer. The setup used in the experiments was slightly different from what the manufacturer had used and so the results for the coupling efficiency are not identical to those of the producer.

Further work in this area could be focused on several different topics. First, the laser diode that is used as the pump source for the SHG crystal could have a better beam quality. The importance of the M^2 value in the frequency doubling could then be addressed. Secondly, the setup that was used could be optimized by experimenting using a fiber to couple the light in the SHG crystal better. Thirdly, the SHG crystal could be non-planar and so have better confinement in the SA- direction. This would allow for higher intensities in the crystal, higher coupling efficiency and overall higher performance of the frequency doubling. This would also require for the laser beam to have a better beam quality in the SA-direction.

REFERENCES

[1] Mishra, U. and Singh, J. *Semiconductor Device Physics and Design*. 1st ed. Includes bibliographical references and index.; ID: alma9910641614405973. Dordrecht: Springer Netherlands, 2008. ISBN: 1-4020-6481-0. DOI: 10.1007/978-1-4020-6481-4.

[2] Svelto, O. *Principles of Lasers*. 5th ed. Includes bibliographical references and index.; ID: alma9910613149005973. New York, NY: Springer US, 2010. ISBN: 1-280-38174-4. DOI: 10.1007/978-1-4419-1302-9.

[3] Coldren, L. A., Corzine, S. W. and Mashanovitch, M. L. *Diode Lasers and Photonic Integrated Circuits*. Vol. 218. Hoboken: John Wiley Sons, Incorporated, 2012. ISBN: 9780470484128.

[4] *Semiconductor Lasers*. https://www.rp-photonics.com/bragg_mirrors.html, Accessed 2021-02-19.

[5] Epperlein, P. W. *Semiconductor laser engineering, reliability and diagnostics a practical approach to high power and single mode devices*. 1st ed. Includes bibliographical references and index.; ID: alma9910683988605973. Chichester, West Sussex, U.K: John Wiley Sons Inc, 2013. ISBN: 1-118-48188-7.

[6] Dimitrijev, S. *Principles of semiconductor devices*. ID: alma9910623473805973. Place of publication not identified: Oxford University Press, 2012. ISBN: 1-62870-172-2.

[7] *Bragg mirrors*. https://www.rp-photonics.com/bragg_mirrors.html, Accessed 2021-08-29.

[8] *Waveguide lasers*. https://www.rp-photonics.com/waveguide_lasers.html, Accessed 2021-08-29.

[9] Uusitalo, T. Single- and Dual-Frequency Laser Diodes based on Surface Gratings. PhD thesis. 2018. URL: https://trepo.tuni.fi/handle/10024/113908.

[10] Zorabedian, P. 8 - Tunable External-Cavity Semiconductor Lasers. Ed. by F. J. Duarte. Tunable Lasers Handbook. San Diego: Academic Press, Jan. 1995, pp. 349–442. URL: https://www.sciencedirect.com/science/article/pii/B978012222695350009X.

[11] *Tapered laser diode*. https://www.rp-photonics.com/tapered_laser_diodes.html, Accessed 2021-08-29.

[12] *Beam divergence*. https://www.rp-photonics.com/beam_divergence.html, Accessed 2021-08-29.

[13] Koechner, W. *Solid-State Laser Engineering*. 6th ed. New York: Springer-Verlag, 2006. ISBN: 9780387290942. URL: https://www.springer.com/gp/book/9780387290942.

[14] *Nonlinear Crystal Materials*. https://www.rp-photonics.com/nonlinear_crystal_materials.html, Accessed 2021-08-29.

[15] Fejer, M. M., Magel, G. A., Jundt, D. H. and Byer, R. L. Quasi-phase-matched second harmonic generation: tuning and tolerances. *IEEE Journal of Quantum Electronics* 28.11 (Nov. 1992). Requirements to be followed when using any portion (e.g., figure, graph, table, or textual material) of an IEEE copyrighted paper in a thesis: 1) In the case of textual material (e.g., using short quotes or referring to the work within these papers) users must give full credit to the original source (author, paper, publication) followed by the IEEE copyright line © 2011 IEEE. 2) In the case of illustrations or tabular material, we require that the copyright line © [Year of original publication] IEEE appear prominently with each reprinted figure and/or table. 3) If a substantial portion of the original paper is to be used, and if you are not the senior author, also obtain the senior author's approval., pp. 2631–2654. DOI: 10.1109/3.161322.

[16] Hum, D. S. and Fejer, M. M. Quasi-phasematching. *Comptes rendus. Physique* 8.2 (2007), pp. 180–198. DOI: 10.1016/j.crhy.2006.10.022. URL: https://dx.doi.org/10.1016/j.crhy.2006.10.022.

[17] Jedrzejczyk, D., Güther, R., Paschke, K., Jeong, W.-J., Lee, H.-Y. and Erbert, G. ötz. Efficient high-power frequency doubling of distributed Bragg reflector tapered laser radiation in a periodically poled MgO-doped lithium niobate planar waveguide. *Optics Letters* 36.3 (2011). J2: Opt. Lett., pp. 367–369. DOI: 10.1364/OL.36.000367. URL: http://ol.osa.org/abstract.cfm?URI=ol-36-3-367.